Collapse of a cylinder of Bingham fluid

Malcolm R. Davidson* N. Hasan Khan*
Y. Leong Yeow*

(Received 7 August 2000)

Abstract

The "Slump Test" is a simple method of measuring the yield stress of certain materials such as concrete and concentrated suspensions. In this procedure a cylindrical test sample is allowed to deform under its own weight, and the yield stress is obtained from the change in height (slump height) of the sample using an empirical calibration curve. In this paper the slump height/yield stress relationship of the material,

*Department of Chemical Engineering, The University of Melbourne, Parkville, Vic. 3052, Australia. mailto:m.davidson@chemeng.unimelb.edu.au

[0]See http://anziamj.austms.org.au/V42/CTAC99/Davi for this article and ancillary services, Published 27 Nov 2000.

considered as a Bingham fluid, is investigated numerically using a finite volume procedure applied to a homogeneous two-fluid (liquid-air) model representing flow of an equivalent single phase with variable properties. Advection is approximated using a van Leer flux limiter to reduce interface smearing without the occurrence of spurious oscillations. Predictions are in reasonable agreement with published experimental data for high yield stress materials, but are less satisfactory when the yield stress is low.

Contents

1 Introduction

Rheologically complex materials such as concentrated mineral suspensions, mud slurries and concrete mixtures exhibit yield stress. The flow behaviour of such materials is dominated by the magnitude of this stress. Mineral suspensions, for example, will not flow in a pipeline if the applied shear stress is everywhere below the yield stress. Conversely, after a heavy downpour, high moisture may cause the yield stress of the topsoil on a mountainside to fall below the shear stress generated by gravitational body force; the soil will then slide down the mountainside as a slurry initiating a mud avalanche. It is therefore important to be able to measure, *in situ* if possible, the yield stress of these materials.

In research laboratories specialised instruments such as the vane instrument and various modified Couette and capillary viscometers [5] are used to measure yield stress on carefully prepared samples. These instruments are either too costly or are not robust enough for general use in the field. Engineers have developed the slump test as a quick and ready means of determining yield stress. In the simplest form of the slump test, a sample of the yield stress material is allowed to deform under its own weight until the final equilibrium shape is reached. The equilibrium shape clearly depends, among other factors, on the yield stress. The objective of the slump test is to extract the yield stress of the material by measuring the difference between the initial and final heights of the sample.

The slump test has the obvious advantage of simplicity; its main drawback is the need of an empirical or semi-empirical calibration curve to convert the observed height change in the sample to a yield stress. From published experimental details on the slump test [6, 8] it is not clear that there is a single well defined calibration curve that is valid for a wide range of yield stresses. Pashias *et al* [6] obtained an algebraic expression for the calibration curve based on an *ad hoc* model of the slump test which they concluded was adequate for the range of materials investigated. However, more recent results [2] seem to indicate that the applicability of this expression is more restricted than originally thought. Schowalter and Christensen [8] analysed the slump test for samples in the shape of truncated cones. As with Pashias *et al* [6], their results also indicate that it is necessary to adopt a more systematic approach to the modelling of the slump test.

The aim of this paper is to predict the slump height/yield stress relationship of a material, considered as a Bingham fluid, by simulating the slump test numerically using a finite volume procedure which treats the slumping fluid and surrounding air as a single fluid with varying properties. The predicted curve is compared with values measured by Pashias *et al* [6] for a variety of materials.

2 Formulation

The transient deformation of the fluid sample is calculated by solving on a fixed grid for the flow of both the liquid and the surrounding air considered together as a homogeneous two-phase mixture (Figure 1). The interface position is determined implicitly at any time by consideration of the volume fraction distribution. This procedure (essentially a Volume-of-Fluid method [3]) is equivalent to solving for the flow of a single phase with variable properties, combined with advection of the volume fraction. The mixture takes the properties of the sample in the liquid phase and those of air in the gas phase, with a volume fraction weighted average in computational cells containing the interface. The precise values of density and viscosity chosen for the gas phase are unimportant.

The governing flow equations for the mixture in this formulation are:

$$\frac{\partial \rho \mathbf{u}}{\partial t} + \nabla \cdot (\rho \mathbf{u}\mathbf{u}) + \nabla p + \rho g \hat{\mathbf{z}} = \nabla \cdot \mu(\nabla \mathbf{u} + (\nabla \mathbf{u})^T) \tag{1}$$

$$\nabla \cdot \mathbf{u} = 0 \tag{2}$$

$$\frac{\partial \theta}{\partial t} + \nabla \cdot (\theta \mathbf{u}) = 0 \tag{3}$$

where $\mathbf{u}$, p, g, μ, θ denote velocity, pressure, gravitational acceleration, mixture viscosity, and sample volume fraction, respectively. The unit vector $\hat{\mathbf{z}}$ is directed upwards. Equation (3) represents continuity of the liquid phase. Combining this with the corresponding continuity equation for the gas phase

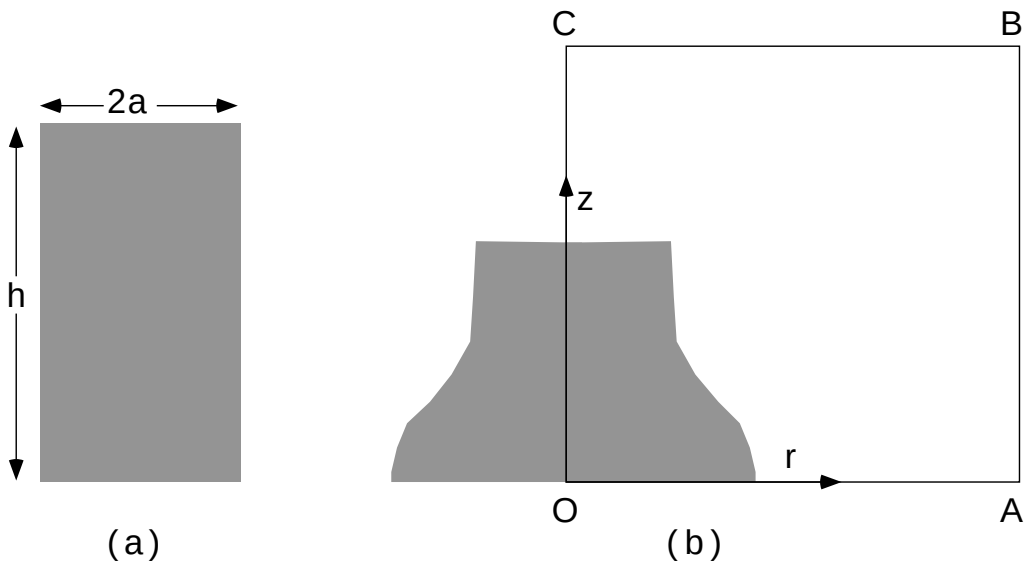

FIGURE 1: Schematic of the flow geometry showing (i) the initial cylindrical sample and (ii) the sample shape at a later time. The computational domain in the (r, z) plane is given by the rectangle OABC

yields Equation (2). Equations (1–3) are typical of those in Volume-of-Fluid formulations (e.g. [7]).

The mixture density ρ is given in terms of the densities of the sample (ρ_l) and the surrounding air (ρ_g) as

$$\rho = \theta\rho_l + (1-\theta)\rho_g \tag{4}$$

The viscosity of the sample is given by

$$\mu_l = \frac{\tau_Y}{\gamma} + \mu_o \tag{5}$$

where γ, τ_Y and μ_o denote the rate of strain, yield stress and plastic viscosity of the Bingham fluid sample, respectively. When $\gamma = 0$, the fluid stress is below the yield stress and the viscosity effectively becomes infinite. Here the dimensionless rate of strain is limited to a minimum value of 10^{-10}. The mixture viscosity in Equation (1) is given in terms of the sample viscosity (μ_l) and the viscosity of the surrounding air (μ_g) as

$$\mu = \theta\mu_l + (1-\theta)\mu_g \tag{6}$$

The governing equations are solved in dimensionless form scaled according to length h (initial sample height), time $\sqrt{h/g}$, density ρ_l, and stress $\rho_l g h$.

With reference to Figure 1, OC is the axis of symmetry and OA is taken to be a no-slip boundary. Since the sample typically consists of slurry of fine

particulates, partial slip on OA may be more appropriate in practice; consideration of this possibility will be made in future work. Zero normal gradient conditions are applied at AB and BC which are chosen to be sufficiently far from the sample so as not to influence the calculation of slumping. For an initial sample aspect ratio $2a/h = 1$, OA and OC are chosen to have lengths of 3 and 1.5 dimensionless units, respectively.

Predictions are made for dimensionless yield stress values ($\tau_Y^* = \tau_Y/\rho_l g h$) in the range $(0.05, 0.4)$ and for a sample aspect ratio of unity, consistent with the data of Pashias *et al* [6].

3 Numerical Considerations

The numerical solution was performed using the commercial fluid flow solver CFX-4.2 [1]. The SIMPLEC algorithm [9] is used to solve for the pressure correction in the mixture flow equations. Advection of the velocity field was performed using the HYBRID differencing scheme, which in this problem becomes (second order) central differencing throughout because the Reynolds number of the flow is very small (less than 0.01 based on properties of the sample). A second order upwind advection scheme with a van Leer flux limiter [4] was used for the volume fraction (Equation (3)) to help maintain the steep gradients of θ in the interface cells without the appearance of spurious oscillations.

Test calculations were performed for two uniform, rectangular computational grids: a coarse grid with 30 and 15 cells in the horizontal and vertical directions, and a finer 60×30 grid. The coarse grid gives a bare minimum of 10 cells over the initial height of the sample. For the coarse grid, we chose the dimensionless time step $\Delta t = 0.001$ for $t < 0.1$ and $\Delta t = 0.01$ thereafter. The Δt values used for fine grid calculations were a factor of 4–10 times smaller. Convergence at each time step was assumed when the normalised sum of the mass residuals was less than 10^{-4}. An under-relaxation factor of 0.1 was applied to iterations of the velocity and volume fraction.

On the coarse grid, reducing the time step by a factor of 2 throughout produced a negligible change in predicted centreline height during the approach of low yield stress materials to the final sample configuration. However, some differences were found in the transient, but not in the final height, when τ_Y^* was increased to 0.3. Differences (2–6%) were found in the final calculated height at still higher yield stresses. Reducing the convergence criterion from 10^{-4} to 10^{-5} produced a negligible effect in all cases.

For a fine grid, predictions of centreline height with time were almost identical to the most accurate coarse-grid predictions at the lowest yield stress $\tau_Y^* = 0.05$. However, some differences were found in the transient, but not in the final height, when τ_Y^* was increased to 0.2. Differences (5–12%) between the final slump height predicted on a coarse and a fine grid were also found for $\tau_Y^* \geq 0.35$. Final results for slump height are based on fine grid calculations for $\tau_Y^* \geq 0.2$.

4 Results and Discussion

Figure 2 shows the predicted variation of centreline height with time. As is expected, the height falls more rapidly and achieves a lower final value as the yield stress of the sample is reduced. In the limit of zero yield stress, the flow is Newtonian and the final height must be near zero as the fluid spreads out over the surface in a thin film. In practice, the calculation of flow with very small yield stress would require a very fine grid to resolve the thin spreading layer on the solid surface.

The predicted height variation with time is insensitive to the choice of plastic viscosity of the Bingham fluid. This occurs because the flow is completely dominated by the yield stress, a circumstance more clearly understood by considering the dimensionless stress-strain ($\tau_l^* - G$) relation for the sample:

$$\tau_l^* = \tau_Y^* + \mu_o^* G \tag{7}$$

where $\mu_o^* = \mu_o/(\rho g^{1/2} h^{3/2})$. In the present calculations τ_Y^*, μ_o^* and G are of order 10^{-1}–1, 10^{-4} and 10^{-2}, respectively, illustrating the dominant role of the yield stress relative to viscosity of the sample.

Figures 3 and 4 show the predicted change in the sample shape as it slumps under its own weight for two different yield stresses. The profiles are derived from the volume fraction distribution at each time. The diffuse band outlining the sample is the region in which the volume fraction is intermediate between one (Bingham fluid) and zero (surrounding air). Obviously the width

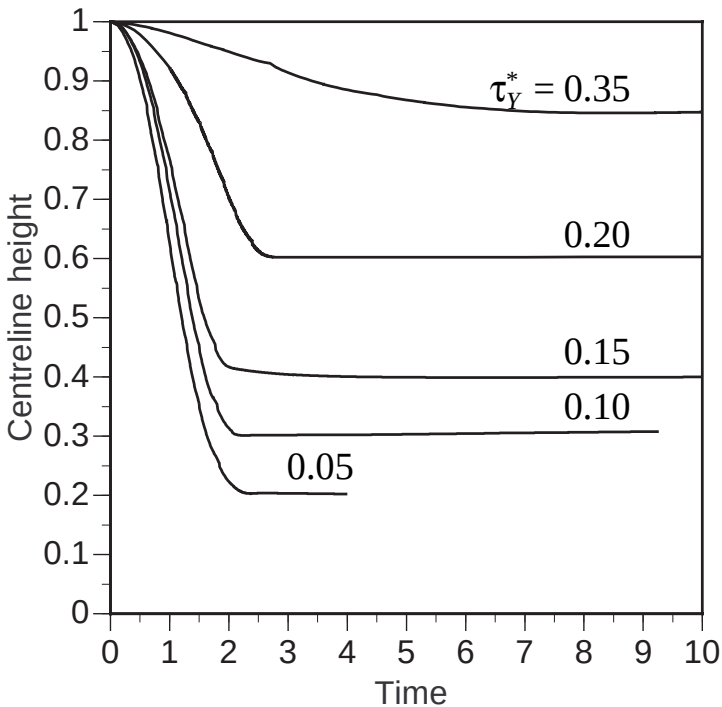

FIGURE 2: Centreline height of the sample vs time for different values of dimensionless yield stress. Height has been scaled by the initial sample height h, and time by $\sqrt{h/g}$.

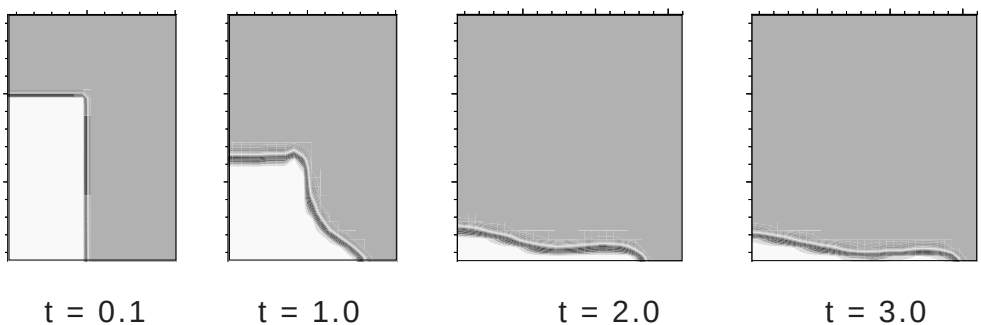

FIGURE 3: Sequence derived from the volume fraction distribution in a fine grid calculation showing the shape change of the sample with dimensionless time when $\tau_Y^* = 0.05$

.

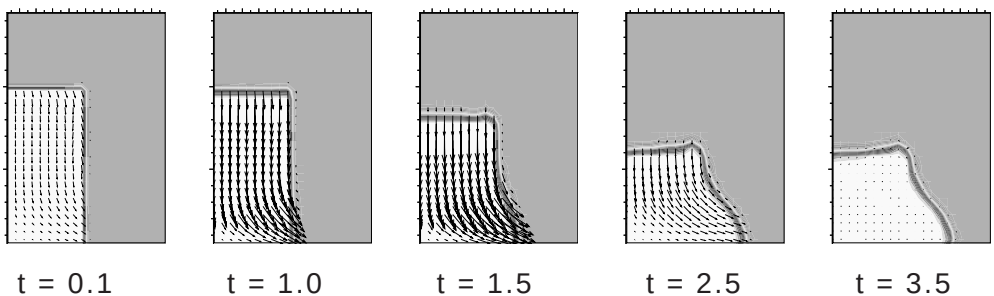

FIGURE 4: Shape change of the sample (derived from the volume fraction distribution in a fine grid calculation) and the velocity vectors with the sample at different dimensionless times when $\tau_Y^* = 0.2$

.

of this band, and hence the definition of the actual interface, depends on the mesh cell size and on the degree of numerical smearing of the interface. The resolution of the profile in Figure 3 where the film is thinnest will be poor as the film thickness approaches that of the mesh cells; however, our numerical tests show that the centreline height (where the film remains thickest) is numerically accurate, at least for $\tau_Y^* = 0.05$. Accurate predictions for lower τ_Y^* values would require a finer computational mesh.

Both Figures 3 and 4 show that the sample begins to collapse almost uniformly across its width. That is, the cylinder collapses as a plug, preserving its topmost shape, with shearing occurring only near the base which grows radially outwards. The predicted shapes are typical of those observed experimentally, including the slight dip which develops in the centre of the top surface for $\tau_Y^* = 0.2$ (Figure 4). The plug-like collapse of the central and top portion occurs because the yield stress is exceeded only near the base and lower side boundary of the cylinder. The effect is more pronounced in Figure 4 because the yield stress is higher than in Figure 3.

The velocity vectors (calculated as $\theta\mathbf{u}$) superimposed on Figure 4 for $\tau_Y^* = 0.2$ show an acceleration of the flow up to $t = 1.5$ followed by a deceleration to zero velocity as shown for $t = 3.5$. The flow patterns show the region of downwards plug flow, which partially diminishes with time, from the bottom and side of the sample as it deforms. Velocity vectors are not shown in Figure 3 but the patterns at $t = 0.1$ and 1.0 are similar to those in Figure 4, only the velocities are larger.

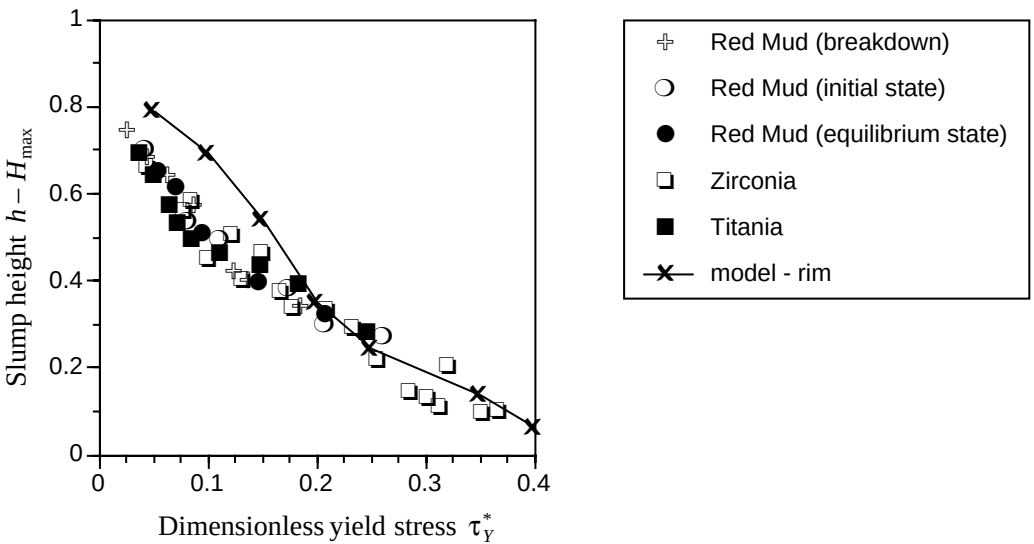

FIGURE 5: Slump height, defined as the difference between the initial sample height h and the maximum final sample height H_{max} vs yield stress. All quantities are dimensionless. The experimental data are those in [6].

Figure 5 shows the predicted slump height variation with yield stress compared with experimental values measured for different materials [6]. The slump height is defined as the difference between the initial sample height and the maximum final sample height. Note that the maximum height is not necessarily equal to the height of the sample at the centreline (see Figure 4). In view of the variability in the data evident in the figure, the agreement between the predicted and experimental values is acceptable for dimensionless yield stress $\tau_Y^* \geq 0.2$, but is less satisfactory for lower values of yield stress. At very low yield stress (Newtonian fluid) the predicted slump height should approach 1. However, the current mesh cannot resolve the thin film which spreads out on the surface when the fluid is almost Newtonian.

Notwithstanding the above discussion, the inability to predict the slump height at very small yield stress is of little practical consequence since the slump test is not used in such cases. Of greater importance is the overprediction of the slump height for $\tau_Y^* < 0.2$ shown explicitly in Figure 5. This overprediction could be a consequence of ignoring surface tension which can play an increasingly significant role in the deformation of the sample as the yield stress is reduced. Surface tension will tend to retard the rate of spreading of the sample. Whether it will also reduce the slump height is not clear. Another factor which will tend to reduce the slump height of the sample, and which is not included in the model, is the effect of removing the sleeve which initially contains the sample. The shear stress imparted by the upwards motion of the sleeve upon removal may be important as the yield stress is reduced. These matters will be investigated in future work.

5 Conclusion

Transient numerical calculations of the the flow of a Bingham fluid deforming under its own weight from an initial cylindrical shape on a horizontal surface have been performed. The calculations are made on a fixed grid for the flow of both the liquid and the surrounding air considered together as a homogeneous two-phase mixture in a procedure similar to Volume-of-Fluid methods. The interface position at any time is determined implicitly from the volume fraction distribution.

The experimentally observed plug-like collapse of the central and top portions of the cylinder is predicted. The final predicted shapes when slumping ceases are also representative of those observed. As is expected, the predicted centreline height falls further and more rapidly with time as the yield stress of the fluid is reduced. The final predicted slump height is acceptable compared with values measured for a variety of yield stress materials when the dimensionless yield stress (scaled by the "hydrostatic" pressure variation over the height of the initial sample) is 0.2 or larger (up to 0.4, the upper range of the experiments). When the yield stress is smaller, the predictions are less satisfactory.

References

[1] AEA Technology. *CFX-4.2 Solver*. Harwell Laboratory, Oxfordshire, UK, 1997. C506

[2] D.V. Boger. personal communication, 1999. C502

[3] J.M. Floryan and H. Rasmussen. Numerical methods for viscous flows with moving boundaries. *Appl. Mech. Rev.*, 42:323–341, 1989. C503

[4] C. Hirsch. *Numerical Computation of Internal and External Flows,* Vol. 2. Wiley Series in Numerical Methods in Engineering, 1995. C506

[5] Q.D. Nguyen and D.V. Boger. Measuring the flow properties of yield stress fluids. *Ann. Rev. Fluid Mech.,* 24:47–88, 1992. C501

[6] N. Pashias, D.V. Boger, J. Summers, and D.J. Glenister. A fifty cent rheometer for yield stress measurement. *J. Rheol.,* 40:1179–1189, 1996. C502, C502, C502, C502, C506, C513, C514

[7] M. Rudman. A volume tracking method for interfacial flows with large density variations. *Int. J. Numer. Methods Fluids,* 28:357-378, 1998. C505

[8] W.R. Schowalter, and G. Christensen. Toward a rationalization of the Slump Test for fresh concrete. *J. Rheol.,* 42:865–870, 1998. C502, C502

[9] J.P. Van Doormaal, and G.D. Raithby. Enhancements of the Simple Method for predicting incompressible fluid flows. *Numerical Heat Transfer*, 7:147–163, 1984. C506